Axisymmetric SCRamjet Engine Design and Performance Analysis

Andreas K. Flock*, Johannes C. Riehmer*, Ali Gülhan†
German Aerospace Center (DLR), 51147 Cologne, Germany

In the present work, we treat the SCRamjet engine as a system, by coupling different analytical design tools. For the intake portion a Busemann tool was used, the combustion chamber was modeled with a one-dimensional reactor, and the nozzle was modeled with the method of characteristics. Performance parameter are discussed while we mainly focus on specific impulse. We used numerical simulations to validate the modeling of the combustion chamber and it turned out that after analytically forcing ignition, the numerical results matched the predictions best. Furthermore, we validated the analytical approach with numerical results and obtained good agreement. According to the analytical tool, for a constant intake pressure ratio of 80 the engine did not ignite at Mach numbers lower than 6 and the specific impulse dropped from 3500 s at Mach 6 to 1200 s and 500 s for Mach 8 and 10, respectively. Due to the small geometry and therefore high friction drag, specific impulse became negative at Mach 11.

Nomenclature

CC	combustion chamber	p	pressure, $[\mathrm{N/m^2}]$
CR	contraction ratio	$\dot{q}$	heat flow, $[\mathrm{J/s}]$
F	force, $[\mathrm{N}]$	s-lip	straight lip geometry
f	fuel to air ratio	SF	outer surface
ff	flow field	str-thr	stream thrust
fi	forced ignition	T	temperature, $[\mathrm{K}]$
h	height, altitude, $[\mathrm{m}]$	t	time, $[\mathrm{s}]$
IN	intake	v	velocity, $[\mathrm{m/s}]$
I_{sp}	specific impulse, $[\mathrm{s}]$	x, y, z	spatial coordinates, $[\mathrm{m}]$
L	length, $[\mathrm{m}]$	δ	truncation angle, $[^\circ]$
LHV	lower heating value	ε	opening angle, $[^\circ]$
$\dot{m}$	mass flow, $[\mathrm{kg/s}]$	η	efficiency
m-av	mass averaged	Θ	temperature ratio
M	Mach number	Π	pressure ratio
NZ	nozzle	φ	equivalence ratio
q	dynamic pressure, $[\mathrm{N/m^2}]$		

Subscript

cc	combustion chamber	st	static
ex	exit	sp	specific
i	internal portion	tr	transition
ig	ignition	∞	free stream condition
o	overall portion		
oa	overall		

I. Introduction

The SCRamjet engine is a potential thrust device for hypersonic aircraft, or access to space vehicles. Because air from the atmosphere is used for the combustion process, no oxygen has to be carried along, and the SCRamjet cycle is generally more efficient, compared to rocket engines [1].

The uninstalled thrust of an engine is calculated by assuming no drag forces on the outer parts of the engine. Furthermore, we will distinguish between viscous drag forces and pressure drag forces. The thrust is often times made

*Research Scientist, Supersonic and Hypersonic Technology Department, Institute of Aerodynamics and Flow Technology, Linder Höhe, 51147 Cologne, Germany
†Department Head, Supersonic and Hypersonic Technology Department, Institute of Aerodynamics and Flow Technology, Linder Höhe, 51147 Cologne, Germany

dimensionless with the mass flow captured by the intake and is then labeled as specific thrust:

$$F_{\mathrm{sp}} = \frac{F}{\dot{m}_0} \tag{1}$$

A parameter, which measures the efficiency of a certain vehicle is the specific impulse:

$$I_{\mathrm{sp}} = \frac{F_{\mathrm{sp}}}{g_0 f} \tag{2}$$

The fuel to air ratio, f, is 34.36 for stoichiometric combustion of hydrogen and oxygen. The specific impulse can be regarded as the intake thrust, divided by the fuel flow rate, that is consumed. This normalized thrust is usually converted with the earth acceleration, g_0, into seconds. Furthermore, the overall engine efficiency is defined as the power delivered by the thrust, divided by the fuel energy released by unit time:

$$\eta_{\mathrm{oa}} = \frac{F v_0}{\dot{m}_{\mathrm{fuel}} LHV} \tag{3}$$

Various analytical studies on the overall SCRamjet engine exist, and in the following a few will be presented: First, in the book by Heiser and Pratt[1], there are various approaches to model the behavior of a SCRamjet engine. Using the first law of thermodynamics and a stream thrust analysis, the general behavior of a SCRamjet engine was modeled. While the results are not necessarily transferable to a practical engine system, we believe that they rather serve the purpose of better understanding the engine behavior and interaction of different variables. Furthermore, a more sophisticated engine analysis is given in the HAP-computer program (Hypersonic Airbreathing Propulsion), which contains frozen flow effects, or a Rayleigh/Fanno flow analysis for example.

Second, in the paper by Smart[2], the engine analysis is used to answer the question of how much compression is needed within a SCRamjet intake. For the intake, an empirical relation is used to relate the kinetic energy efficiency to the Mach number ratio within the intake. In other words, the quality of the compression - the efficiency - is related to the quantity of compression - the reduction in Mach number. The combustor was capable of operating in dual mode, and is described in more detail in[3]. Finally, the nozzle was set to a certain contraction ratio and a fixed nozzle efficiency was used to reduce the total pressure within an otherwise isentropically expanding nozzle.

Third, in a single-stage-to orbit conceptual study, Billig investigated the SCRamjet as a system by using databases and analytical means to extract engine parameter[4]. The intake performance was approximated by a quadratic equation, that related the intake contraction and compression ratio to the flight Mach number. The combustor and nozzle performance were calculated by analytical relations that contained respective efficiencies.

In the present paper, we treat the SCRamjet engine as a system, while bringing together several tools and experiences gained in previous studies[5,6]. A schematic overview of the different tool-modules as well as of the input or boundary conditions, which need to be fed into the tool, is provided in figure 1. Furthermore analytical results are presented for varying flight Mach numbers. Finally we compare some engine configurations to numerical simulations performed with the DLR solver TAU.

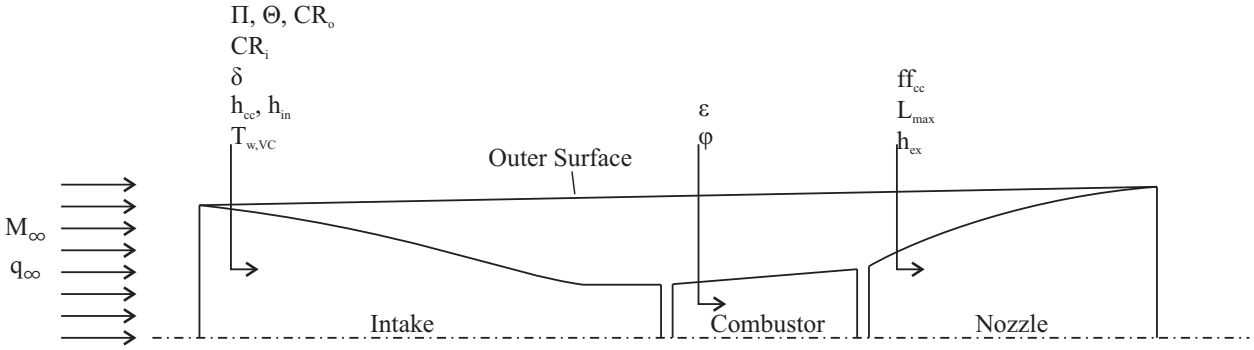

Figure 1. Sketch of generic SCRamjet along with input parameters for geometry generation.

II. Methods and Materials

The design loop is schematically displayed in figure 2. The inflow conditions were fed into the intake tool, which iterated until the desired pressure ratio was reached. Next, the intake exit conditions were forwarded to the combustor tool, which was coupled with the nozzle design program and the tool that modeled the outer surface of the engine. Finally, the engine performance parameter were extracted. In the following, we will describe the individual tools in more detail and we will explain the flow solver TAU, which was used for further analysis.

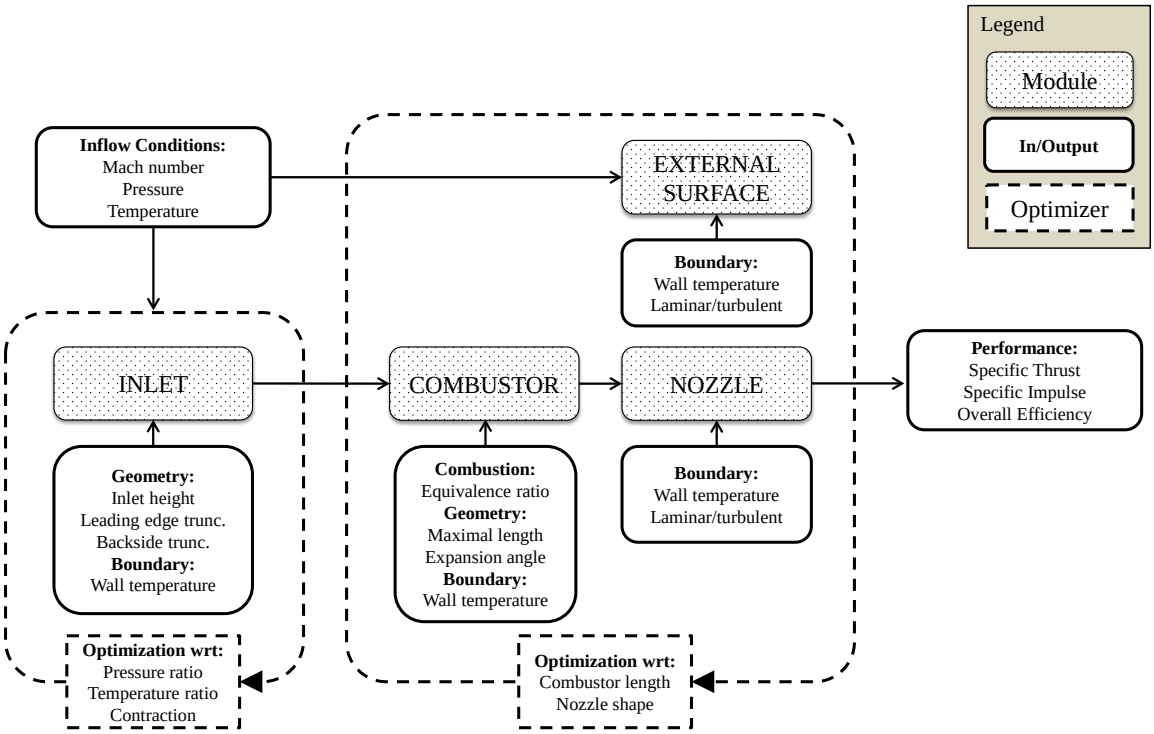

Figure 2. Block diagram of generic SCRamjet engine design loop.

A. Intake Module

We used a Busemann intake as the compression system, and a schematic image is displayed in figure 3. In a classical Busemann intake, air is isentropically compressed, starting at a 0 deg inflow leading edge. At the rear end of the Busemann intake, a conical shock forms after which the flow is homogeneous again. Because in theory this conical shock is the only source of total pressure loss and because the shock occurs at the lowest Mach number, Busemann intakes usually have very high performance characteristics. The classical Busemann flow field is described by the Taylor – McColl equations, and further information can be found in[7,8]. Nevertheless, because these intakes tend to become long and because they have a large amount of internal contraction, their practical usage is critical.

The following three changes were made to the classical Busemann geometry:

1. To reduce intake length, we truncated the Busemann intake at the leading edge. To accommodate the changes to a classical flow field, we modeled the pressure increase at the leading edge with an oblique shock and further adjusted the pressure at the rear end, to adjust the mass flow, going through the intake.

2. To further reduce intake length, and to impose a certain amount of non homogeneity to the intake exit flow, we were able to also truncate the intake at the rear side. The change in flow properties at the rear side was modeled with a stream thrust analysis.

3. To accommodate for viscous effects, we used a viscous correction[6,9,10]; therefore, we calculated various boundary layer properties, such as displacement thickness or skin friction along the Busemann intake contour for the inviscid pressure distribution. With the displacement thickness we widened the Busemann geometry to accommodate for the additional contraction by the boundary layer and with the skin friction, we calculated the viscous forces along the intake wall. With these viscous forces we were able to calculate performance parameter, such as total pressure recovery, or a Mach number and temperature, which are valid for viscous flow.

The Taylor – McColl equations, and the previously described changes were incorporated in a FORTRAN 95 program, which was compiled on a Linux workstation. To automate the usage, a python routine was written, which could execute a desired number of simulations. Calculation times for the intake tools were on the order of minutes. The Busemann geometry was written into a file, which could be automatically post processed with the grid generator, while critical geometry values and intake parameter were fed into the combustion chamber tool.

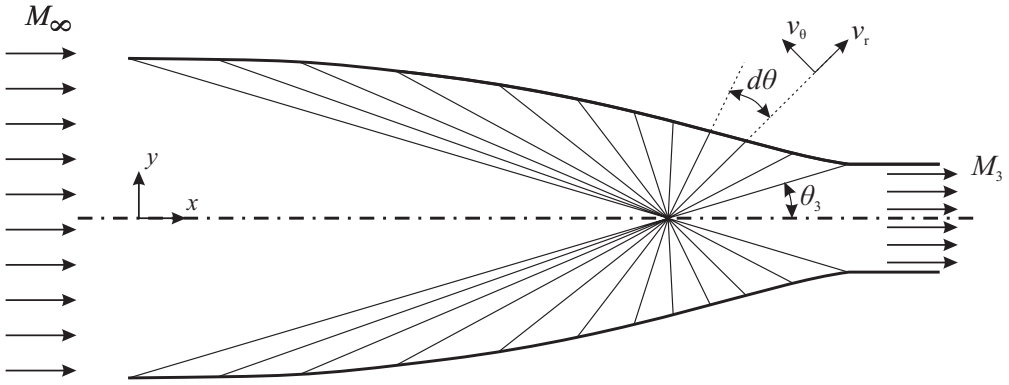

Figure 3. Schematic geometry of a classical Busemann intake.

B. Combustor Module

The combustor was modeled with a circular duct with area change and the duct diameter at the entrance was taken from the intake geometry. Furthermore, we used intake exit pressure, temperature and Mach number as the combustion chamber entrance conditions. Next, we integrated along the combustion chamber length, to calculate the change in flow properties. To go from one integration step (i) to the subsequent one ($i + 1$) (see also figure 4), the following steps were performed:

1. The increase in total enthalpy was calculated with an isochoric reactor modeled with the open source chemical kinetics software Cantera[11] for a certain time step, which could be transformed into a certain length via the flow velocity. The combustion model of Jachimowski[12] was used, but also other models like GRI-Mech[13] could easily be integrated. The resulting increase in energy, calculated with Cantera, was reduced by the heat loss into the walls, calculated with a given friction coefficient and the Reynolds analogy.

2. The heat release was used in the Rayleigh equations[14], to calculate a change in Mach number, temperature and pressure. In case of chocking the equivalence ratio is reduced from 1.0 sequentially to 0.0 in steps of 0.1.

3. Furthermore for the incremental distance $\mathrm{d}x$, the influence of friction and area change was considered. A more detailed treatment of flow with friction and area change is given in[15].

In a SCRamjet the ignition delay time strongly depends on internal flame holders and other ignition devices which create local hot spots. This can not be modeled with this model directly. We tried to vary the ignition delay time of the combustion by creating free radicals which trigger the reaction. To determine the right chemical composition, which gives us a lower ignition delay time, we started two separate isochoric reactors with different temperatures, one with the mean temperature at the combustor entrance and one with the temperature of local hot spots. The mass fraction of water was used as a trigger to determine the start of the reaction and a threshold of 0.001 was used. In figure 5, a schematic visualization of the mechanism is shown with a combustor temperature of 800 K and an ignition temperature of 1500 K. By this method the ignition delay time could be reduced, while the combustion time and efficiency changed only marginally.

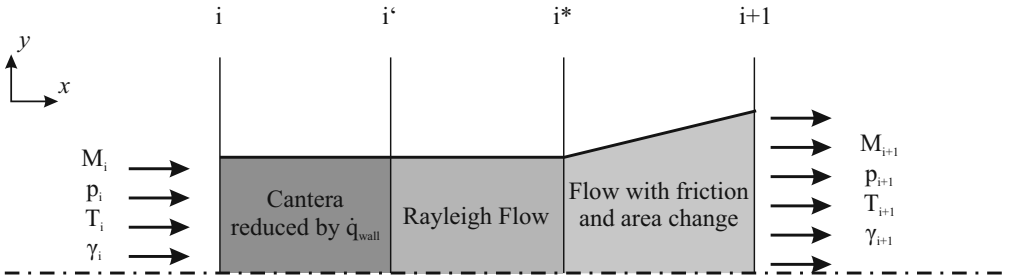

Figure 4. Schematic setup of the combustion chamber modeling.

C. Nozzle Module

The nozzle geometry was designed with the method of characteristics for axisymmetric flow. Detailed information on the method of characteristics can be found in[8,16,17]. The combustor exit Mach number and the heat capacity ratio were

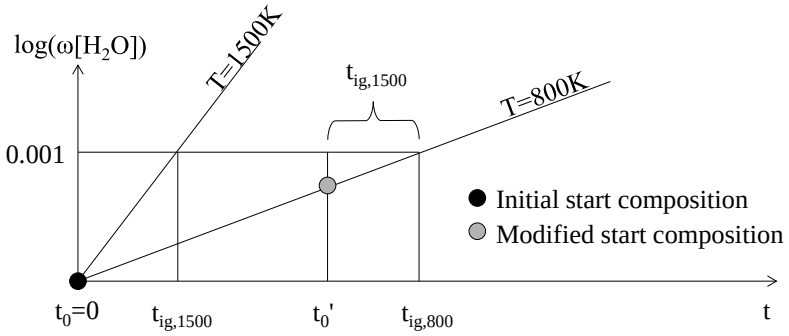

Figure 5. Water content plotted versus time for the regular and forced ignition case.

used as the nozzle entrance condition for the initial isentropic flow field. This means a frozen flow in the nozzle was assumed. For consideration of friction forces a constant skin friction coefficient, taken from the combustor, was used. By integration of the pressure and friction forces, the total thrust of the nozzle was calculated along the surface. To get the optimal thrust, a whole set of configurations with different combustor lengths, initial nozzle expansion ratio and nozzle truncation was calculated. By summation of the forces of the inlet, the combustor, the nozzle and the generated outer surface the whole engine thrust for each configuration was calculated. The configuration, which delivers the maximum thrust was chosen as optimum for the specified inlet and combustor settings.

D. Outer Flow Path

The outer flow path was approximated with a straight line connecting the inlet leading edge and the trailing edge of the nozzle, and had the shape of a truncated cone. To calculate the surface pressure, the oblique shock equations were used in case of a positive angle of attack and the Prandtl-Meyer-equations for a negative value. The friction forces were calculated with the reference temperature method by [18]. As transition is expected on the outer surface, a transition Reynolds number was calculated with the following formula [19] and switched from laminar to turbulent accordingly.

$$Re_{\mathrm{tr}} = 10^{6.421\exp(1.20910^{-4}M^{2.641})} \tag{4}$$

Again the forces where calculated by integrating the finite forces over the running length.

E. Engine Design Margins and Boundary Conditions

We used Hydrogen as fuel and assumed that fuel and air were perfectly mixed at the combustion chamber entrance. For constant dynamic pressure trajectories of $q_\infty = 0.5$ bar, atmospheric conditions were extracted from the standard atmospheric tables [20]. The investigated Mach numbers varied from $6, 8, 10, 12$ to 14 and the free stream pressure and temperature along the constant dynamic pressure trajectory are summarized in table 1. The intake capture area was constant and the radius was 0.11 m. A plot of mass flow versus altitude and Mach number is given in figure 6.

Table 1. Free stream conditions and altitude along constant dynamic pressure trajectory.

M	6	8	10	12	14
p [Pa]	2080.0	1170.0	748.0	520.0	382.0
T [K]	222.9	226.7	231.4	238.5	244.6
h [km]	26.2	30.0	33.0	35.5	37.7

As reference conditions, we used the Mach 8 configuration at a constant static pressure ratio of 120. To force ignition and reduce ignition delay time, an artificial temperature of 1500K in the combustor was assumed. The reference wall temperature and equivalence ratio were 300 K and 1, respectively. We note that the low wall temperature was used, to reduce ignition within the boundary layer during the numerical simulations. If one of the reference condition was varied, the other ones were held constant, if not stated otherwise; for the Mach number variation, for example, the intake pressure ratio, the wall temperatures and equivalence ratios were held constant.

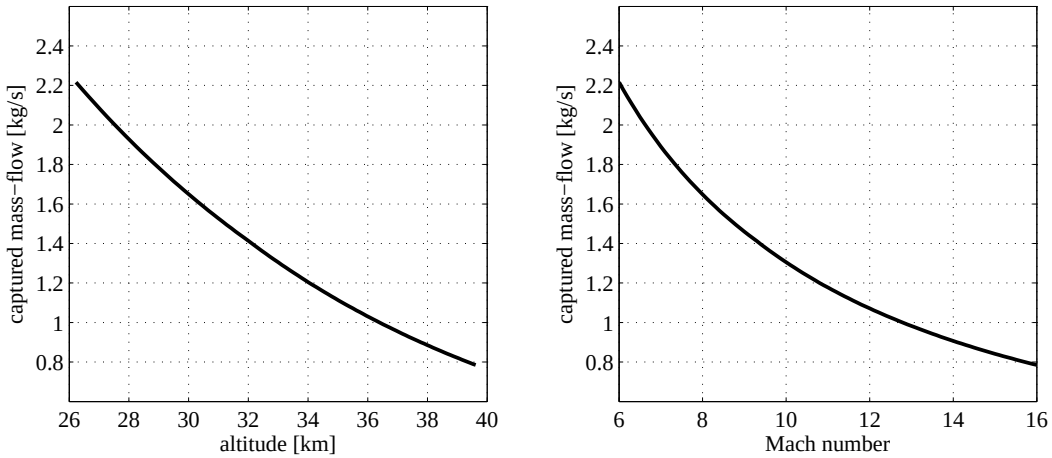

Figure 6. Mass flow through engine, plotted versus altitude (left) and Mach number (right) for constant, circular capture area with $r = 0.11$ m.

F. Numerical Approach

In addition to the analytical modeling and design of the SCRamjet geometry, we performed numerical simulations, to validate the analytical results. We used the finite volume DLR-TAU flow solver[21] with a two-equations turbulence model ($k-\omega$ SST)[22]. Inviscid fluxes were reconstructed with a second order upwind scheme.

Combustion was also modeled with a Jachimowski scheme according to the simplified combustion chamber[12]. Each module: inlet, combustor, nozzle and outer surface could be simulated separately and the interfaces were interpolated between the individual sections. All wall boundary conditions were at constant temperature, which could be modified for each module. The boundary layer was assumed turbulent except for the outer surface which was modeled transitional and the transition location was set according to equation (4).

A hybrid grid was used with an average size of 50000 cells for the inlet, 50000 cells for the combustor, 20000 for the nozzle and 20000 cells for the outer surface. The boundary layer was resolved with a structured grid with approximately 30 cells in height and $y+ < 1$ was assured by further reordering the structured sub layers. The simulation was scripted and computation times ranged from 3 to 12 hours depending on the simulated case.

III. Results

In the present section, first the combustion chamber is validated by comparing analytical predictions to numerical simulations of a duct with a reacting flow field. Furthermore purely analytical results are displayed and finally some conditions are directly compared to results from numerical simulations.

A. Combustion chamber validation

To validate the modeling of the combustion chamber, we compared analytical results for a certain combustion chamber condition with numerical simulations (figure 7). The reference condition was extracted from the stream thrust averaged exit conditions of the inlet and resulted in a combustor entrance Mach number of 3.2, a temperature of 1026 K and a pressure of 95000 Pa. As can be seen in figure 7, no ignition occurred in the CFD simulations for Euler walls, as well as in the analytical tool. After applying the forced ignition mode in the analytical tool, combustion occurred at $x = 0.05$ m and was completed at around $x = 0.2$ m. To compare these values with numerical simulations, first a simulation with constant inflow condition was performed which showed ignition start and end at $x = 0.5$ m and $x = 0.8$ m, respectively. Second, the exit conditions of the inlet were interpolated on the entrance conditions of the combustor, which gave a inhomogeneous flow and created an instant combustion at the combustor entrance. The numerical simulations show the strong dependency of the inflow uniformity on the combustions process itself and validated our ignition model. All combustion cases give a comparable temperature rise which indicates the validity of the analytical approach.

B. Analytically Calculated Engine Behavior

In figure 8 we displayed the SCRamjet geometries designed for the different Mach numbers. The intake was truncated at the leading edge with 4 deg and the intake compression ratio was $\Pi_{\mathrm{st}} = 80$. The combustion chamber cross sectional area was held constant, and its length was automatically calculated in the combustor/nozzle/external-surface

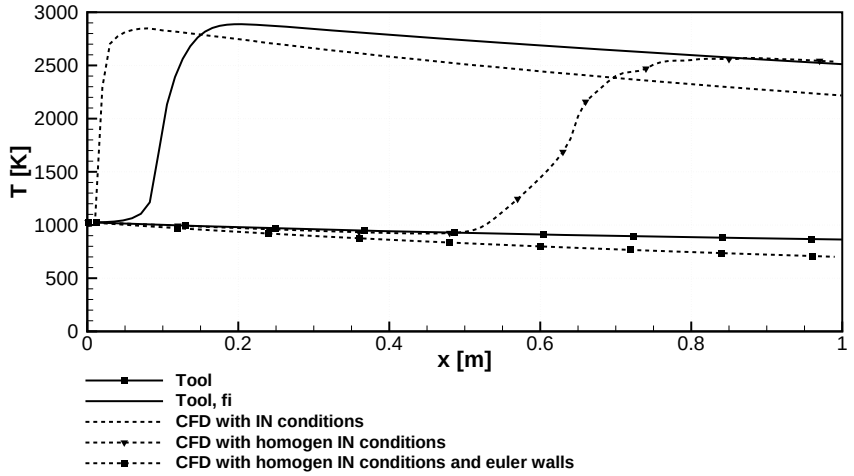

Figure 7. Static temperature distribution in the combustion chamber, plotted versus combustor legnth calculated analytically and with CFD; intake pressure ratio was at 80, and combustion chamber opening angle was at 1 deg.

optimization loop. The intake length increased with higher Mach numbers, and while the capture area was held constant, one could see only little change in combustion chamber diameter. Combustion chamber lengths initially increased until Mach 10, and then decreased again. At Mach 14 the optimization tool reduced the combustor length to a minimum value, because thrust could no longer overcome drag. The nozzle length was approximately constant. Furthermore, the combustion chamber static temperature was plotted versus the length, and one can see the increase in static temperature at the combustor entrance with increasing Mach number.

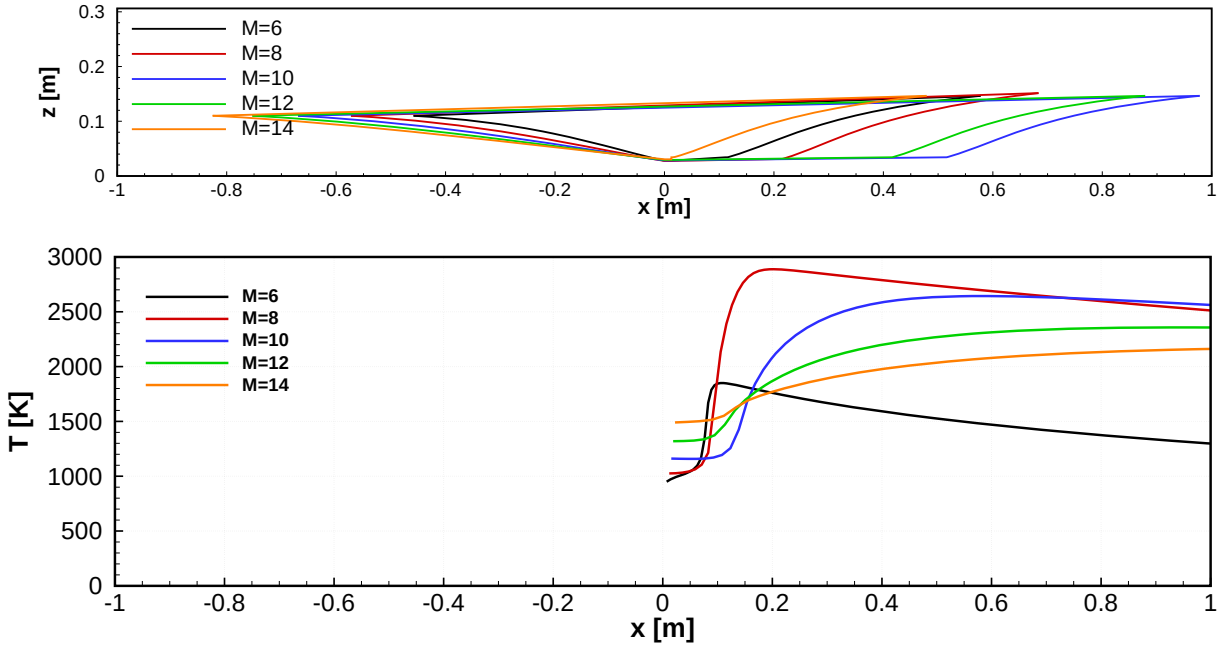

Figure 8. SCRamjet geometries designed for reference conditions at different Mach numbers.

In figure 9 (left), specific impulse was plotted versus flight Mach number for a constant intake pressure ratio of 80. Starting at the reference condition ($M = 8$), on the one hand, the dynamic pressure was held constant, and on the other hand, the flight altitude was held constant. The combustor ignited with forced ignition turned on down to Mach numbers of 6.5 and 6 for the $p_\infty = const.$ and $q_\infty = const.$ case respectively. Generally with increasing dynamic pressure the specific impulse was larger; however the engine will have to sustain higher heat loads.

We also investigated the influence of the engine size and results are displayed as I_{sp} versus M in figure 9 (right). Generally, with increasing engine size, the Reynolds numbers will increase and viscous effects will decrease. Therefore, friction drag, compared to total drag, will be lower, which can be seen by the higher specific impulse for larger engine geometries.

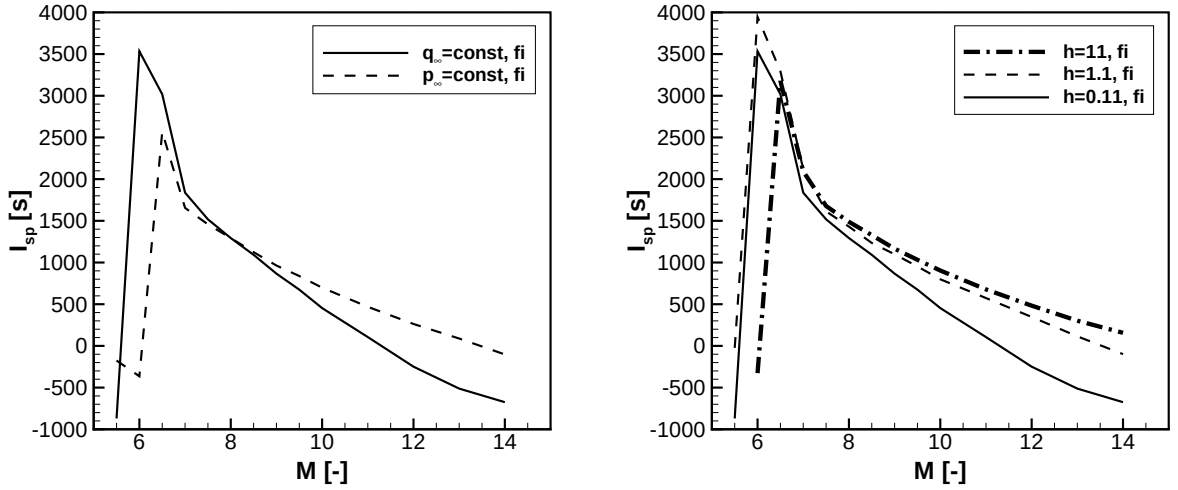

Figure 9. Specific Impulse vs Mach number for constant dynamic pressure and constant altitude (left) and varying geometry size (right).

In figure 10 (left), specific impulse is plotted vs Mach number for different intake compression ratios. Furthermore, we plotted it versus the pressure ratio for different Mach numbers 10 (right). Generally for increasing intake pressure ratio, the specific impulse improved. When plotted versus intake pressure ratio, specific impulse seemed to settle at a constant value, but we expect that there is a maximum, and that specific impulse will decrease above a certain intake pressure ratio. We furthermore note, that at very high intake pressure ratios we encountered flow separation during the numerical simulations and also sometimes in the integral method which was used for the viscous correction within the intake.

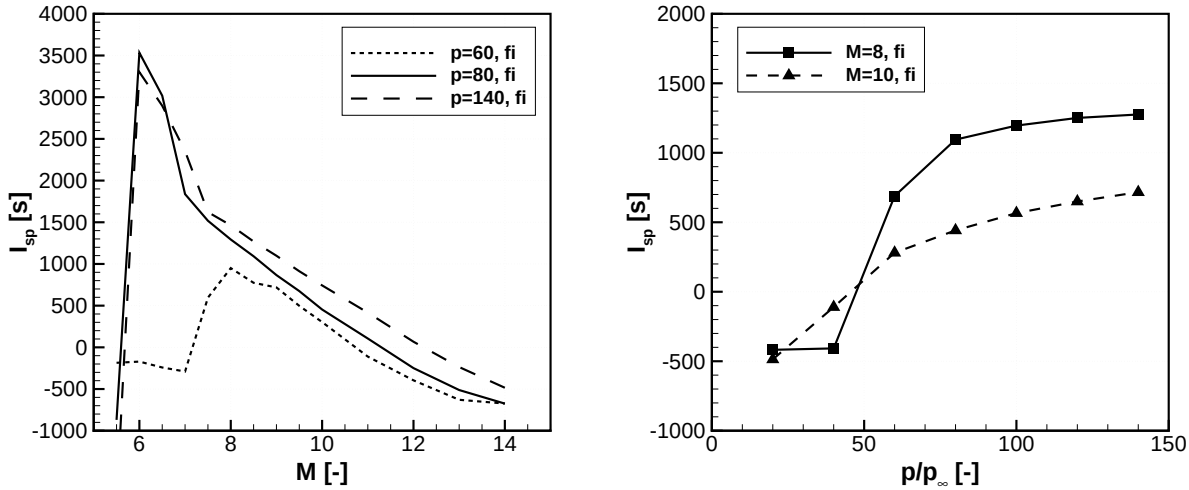

Figure 10. Specific impulse plotted vs Mach number for varying intake pressure ratio (left) and plotted vs intake pressure ratio for different Mach numbers (right).

In the left graph of figure 11 the specific impulse for different equivalence ratios for the reference configuration is plotted. A peak of $1700\,\mathrm{s}$ was observed at an equivalence ratio of 0.5 and for lower ratios the specific impulse decreased strongly and for values smaller than 0.2 negative values were observed. For values higher than 0.5 the specific impulse was also slowly decreasing. We assume the reason for this decrease is the increasing gas temperature in the combustor, which leads to dissociation and therefore to a loss of combustion energy.

We also investigated the wall temperature influence on the performance and varied it between $300\,\mathrm{K}$ and $2000\,\mathrm{K}$ for the natural and forced ignition. Thereby the $300\,\mathrm{K}$ condition was also used as reference condition and corresponds to a cold wall case, which can be observed when a SCRamjet is started. From the right graph in figure 11 it can be observed, that for the natural ignition case the specific impulse increased with higher wall temperatures. The reason for this is the lower energy absorption of the wall for higher temperatures, which could then be used to increase the engine thrust. It is also obvious that for wall temperatures between $1200\,\mathrm{K}$ and $1500\,\mathrm{K}$ the temperature in the combustor

was high enough to enable natural combustion. The right graph in figure 11 shows the data for forced ignition which showed the same behavior, except that for lower wall temperatures ignition could still be observed. There was a difference between the natural and forced ignition for higher wall temperatures which was not expected and it was assumed that these lines would merge for ignition case. We assume the reason that the natural ignition results in lower specific impulse in comparison to forced ignition is that natural combustion requires longer combustors and therefore create more friction and heat losses in the combustor.

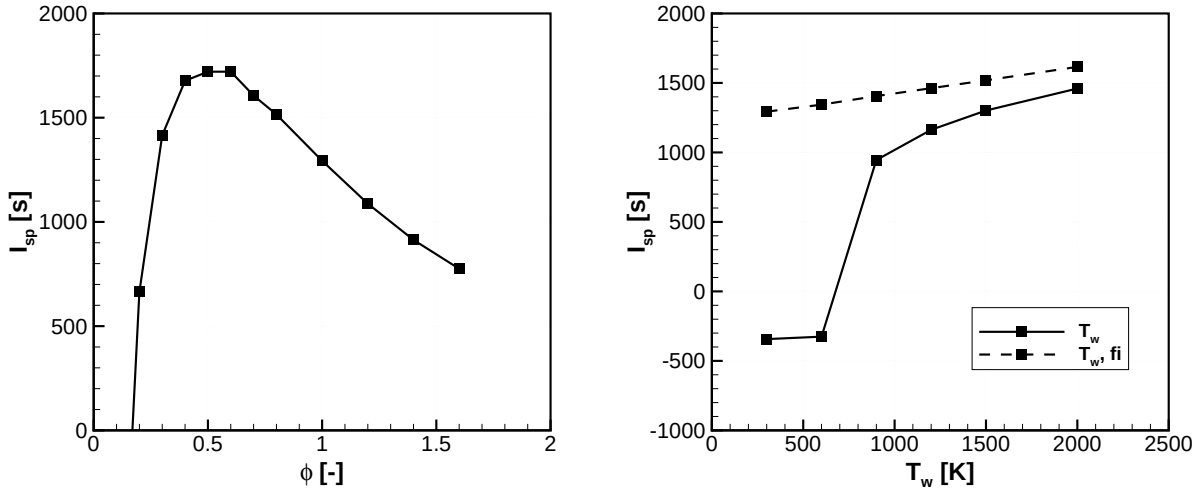

Figure 11. Specific impulse for varying equivalence ratio (left) and varying wall temperature (right).

C. Detailed Reference Condition Performance

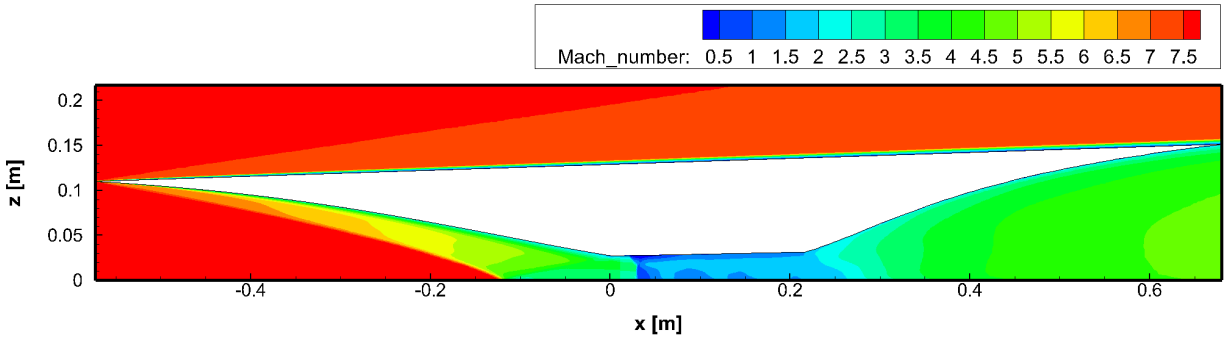

Figure 12. Mach number contour for reference condition at Mach 8; for detailed performance characteristics see table 3.

.

In table 2 the individual forces and the different specific impulses which each individual component created, derived from the analytical tool for forced ignition, are listed for $M_\infty = 8$. We choose the forced ignition case because natural ignition was not observed for the selected parameter.

A first observation of this table was an uninstalled specific impulse of this configuration of $1293\,\mathrm{s}$ and even a higher value of $1752\,\mathrm{s}$ if viscous forces would be absent. Taking into account the forces generated by the outer surface these values dropped by approximately 10%. The forces generated by viscous drag were very high and reduced the total thrust by approximately 30%. Thereby each module produced comparable viscous drag.

Comparing the results from the design tool from table 2 with the numerical results in table 3 a drop of the specific impulse on the order of 20% was observed. In summary:

- The tool under predicted the forces generated by the inlet.
- The numerical simulation of the combustor created a much higher thrust, which was caused by a faster ignition of the numerical combustor (see figure 7).

Table 2. Design/Analytical thrust and specific impulse for fully axisymmetric SCRamjet reference configuration for $M_\infty = 8$.

	F_x[N]					I_{sp}[s]	
	IN	CC	NZ	SF	total	installed	uninstalled
total	414	−46	−970	92	−510	1095	1293
inviscid	324	−102	−1038	57	−759	1630	1752
friction drag	90	56	68	35	249	–	–

- The nozzle produced less thrust during the numerical simulation because part of the thrust was already produced in the combustor.
- The outer surface matched quite well with the analytical approach.

The performance values calculated for the individual engine components showed relatively high differences between the two approaches. By summing up the individual components these deviations partially canceled out.

Table 3. CFD thrust and specific impulse for fully axisymmetric SCRamjet reference configuration for $M_\infty = 8$.

	F_x[N]					I_{sp}[s]	
	IN	CC	NZ	SF	total	installed	uninstalled
total	474	−135	−858	92	−427	918	1115
inviscid	354	−176	−954	53	−723	1553	1668
friction drag	120	41	96	39	296	–	–

In figure 13 (left) we plotted the specific impulse versus the flight Mach number for the analytical results and numerical simulations. The engine was designed for the reference condition with an intake compression ratio of 80, a truncation angle of 4 deg, and a combustion chamber opening angle of 1 deg. At Mach numbers lower than 6, the analytical tool did not ignite even though the forced ignition mode was turned on. The edge at $M \approx 7$ is caused by the decrease in equivalence ratio, which needed to be used to avoid chocking. This increased the specific impulse, which for Mach 8 had a maximum I_{sp} of 1700 s at an equivalence ratio of ≈ 0.5. Furthermore, in figure 13 (right), the difference between installed versus uninstalled I_{sp} and the effect of friction on specific impulse can be observed.

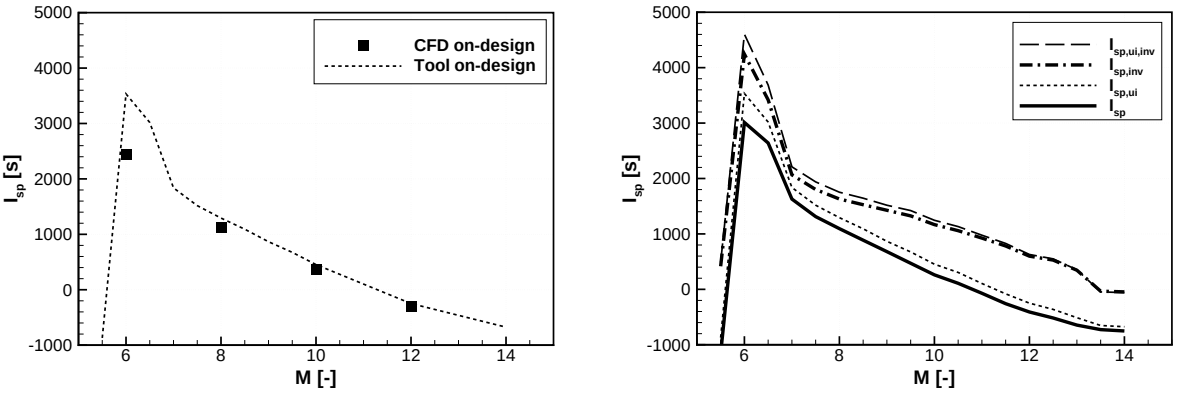

Figure 13. Specific impulse of reference condition, calculated analytically with forced ignition turned on and with DLR-TAU (left) and uninstalled as well as installed specific impulses (right);

IV. Conclusion

In the present paper we presented an approach to model and link different SCRamjet engine components, to ultimately estimate the SCRamjet engine performance. Purely analytical tools were used, with which we could calculate

a generic engine geometry and which had run times on the order of minutes. Results were validated with the DLR finite volume solver TAU for a couple of conditions and generally the calculated specific impulses matched well. The main conclusions include:

1. For the combustion chamber modeling we used a one-dimensional reactor with attached Rayleigh flow and flow with friction and area change. Furthermore, a forced ignition mode was added, to match the numerical results better. The modeling was validated by comparing it to CFD simulations with DLR-TAU of a reacting flow field.

2. Between Mach 6 and 14, the engine geometry length was on the order of $2\ \mathrm{m}$, while the intake capture area was held constant ($r_{\mathrm{in}} = 0.11\ \mathrm{m}$). For Mach numbers lower than 6, no ignition happened, even when the forced ignition mode was turned on. Specific impulse ranged between $3500\mathrm{s}$ and $500\mathrm{s}$ for Mach 6 and 10, respectively and became negative at $M = 11$, because the relatively low-sized vehicle could no longer overcome drag.

3. While varying the equivalence ratio at a constant Mach number of 8, we observed a maximum in specific impulse of $1700\mathrm{s}$ for $\varphi = 0.5$.

4. For constant Mach number, specific impulse increased with increasing engine size and increasing wall temperature.

Acknowledgments

The present work was funded during the Research Training Group 1095/2 (2005-2014). We would like to thank the German Research Foundation (DFG) for the support during that period.

References

[1]Heiser, W. H. and Pratt, D. T., *Hypersonic Airbreathing Propulsion*, AIAA Education Series, 1994.

[2]Smart, M. K., "How Much Compression Should a Scramjet Inlet Do ?" *AIAA Journal*, Vol. 50, No. 3, 2012, pp. 610–619.

[3]Smart, M. K., "Scramjets," *The Aeronautical Journal*, , No. 3219, 2007, pp. 605–619.

[4]Billig, F. S., "Design and Development of Single-Stage-to-Orbit Vehicles," *John Hopkins APL*, Vol. 11, No. 3, 1990, pp. 336–352.

[5]Riehmer, J. C. and Gülhan, A., "Design of a Scramjet Nozzle with Streamline Tracing Technique and Reference Temperature Methode," *7th Aerothermodynamics Symposium on Space Vehicles*, 2011.

[6]Flock, A. K. and Gülhan, A., "Viscous Effects and Truncation Effects in Axisymmetric Busemann SCRamjet Intakes," *53rd Aerospace Sciences Meeting*, 2015, pp. 1–15.

[7]Mölder, S. and Szpiro, E. J., "Busemann Inlet for Hypersonic Speeds," *AIAA Journal*, Vol. 3, No. 8, 1966, pp. 1303–1304.

[8]Anderson, J. D. J., *Modern Compressible Flow*, McGraw Hill, 1990.

[9]Smart, M. K., "Design of Three-Dimensional Hypersonic Inlets with Rectangular-to-Elliptical Shape Transition," *Journal of Propulsion and Power*, Vol. 15, No. 3, May 1999, pp. 408–416.

[10]Wie, D. M. V. and Mölder, S., "Applications of Busemann Inlet Designs for Flight at Hypersonic Speeds," *AIAA Journal*, 1992.

[11]Goodwin, D. G., Moffat, H. K., and Speth, R. L., "Cantera: An Object-oriented Software Toolkit for Chemical Kinetics, Thermodynamics, and Transport Processes," Tech. rep., 2014.

[12]Jachimowski, C. J., *An Analysis of Combustion Studies in Shock Expansion Tunnels and Reflected Shock Tunnels*, Citeseer, 1992.

[13]Smith, G., Golden, D., Frenklach, M., and Eiteener, B., "GRI-Mech 3.0," Tech. rep., 2000.

[14]Zucrow, M. J. and Hoffman, J. D., *Gas Dynamics Volume I*, John Wiley & Sons, 1976.

[15]Oosthuizen, P. H. and Carscallen, W. E., *Compressible Fluid Flow*, McGraw Hill, 1997.

[16]Yu, Y.-N., "A Summary of Design Techniques for Axisymmetric Hypersonic Wind Tunnels," Tech. Rep. November 1958, 1958.

[17]Cronvich, L. L., "A Numerical-graphical method of characteristics for axially symmetric isentropic flow," *Journal of the Aeronautical Sciences*, Vol. 15, No. 3, 1948, pp. 155–162.

[18]Meador, W. E. and Smart, M. K., "Reference Enthalpy Method Developed from Solutions of the Boundary Layer Equations," *AIAA Journal*, Vol. 43, No. 1, 2005, pp. 135–139.

[19]Bowcutt, K. G., Anderson, J. D., and Capriotti, D., "Viscous Optimized Hypersonic Wavers," *AIAA 25th Aerospace Sciences Meeting*, 1987.

[20]Unknown, "The U.S. Standard Atmosphere," Tech. rep., U.S. Government Printing Office, 1976.

[21]Mack, A. and Hannemann, V., "Validation of the Unstructured DLR-TAU-Code for Hypersonic Flows," *32nd AIAA Fluid Dynamics Conference and Exhibit*, No. June, 2002.

[22]Menter, F. R., Kuntz, M., and Langtry, R., "Ten Years of Industrial Experience with the SST Turbulence Model," *Heat and Mass Transfer*, Vol. 4, 2003.